2009-01-3162

Advanced Electrical Signature Analysis of Aircraft Electrical Generators

Freeman Rufus Jr., Seungkoo Lee and Ash Thakker
Global Technology Connection, Inc.

Sean A. Field and Nathan Kumbar
NAVAIR

ABSTRACT

The electrical and mechanical failures (such as bearing and winding failures) combine to cause premature failures of the generators, which become a flight safety issue forcing the crew to land as soon as practical. Currently, diagnostic / prognostic technologies are not implemented for aircraft generators where repairs are time consuming and its costs are high. This paper presents the development of feature extraction and diagnostic algorithms to ultimately 1) differentiate between these failure modes and normal aircraft operational modes; and 2) determine the degree of damage of a generator. Electrical signature analysis based features were developed to distinguish between healthy and degraded generators while taking into account their operating conditions. The diagnostic algorithms were developed to have a high fault / high-hour detection rate along with a low false alarm rate. The feature extraction and diagnostic algorithms were evaluated against P-3 generator data (phase voltages / currents) collected at various loads and operating line frequencies for healthy, low-hour and high-hour generators. The results show that the electrical signature analysis of the generator's phase voltage(s) can be used to detect and track its health.

INTRODUCTION

The P-3 Navy aircraft uses a Bendix (later AlliedSignal and currently Honeywell) generator that was designed over 30 years ago. The P-3 generator is a salient 8-pole (8 rotor bars), 6,000-rpm, 3-phase brushless ac generator. The running speed of the generator is 5700 rpm to 6,300 rpm (line frequency of 380 Hz to 420 Hz). The rated voltage and power is 115 VAC and 60 kVA (20 kVA/phase), respectively. It has a 12-pole ac exciter and a three-phase, half-wave diode rectifier rotating with the exciter armature and main generator field assembly. A single-phase permanent magnet generator (PMG) furnishes control voltage and power for the voltage regulator.

The electrical and mechanical issues (due to being continuously operated beyond design point and less than optimal drive end bearing support) combine to cause premature failures of the P-3 generators. Repairs are time consuming and its costs are high. Currently, diagnostic / prognostic technologies are not implemented for P-3 generators and other electrical power systems. Although some time series data (such as phase voltage and current) are collected during ground testing, no time series data is collected in-flight for the generators. Figure 1 shows the disassembled parts of a brushless ac generator for the P-3.

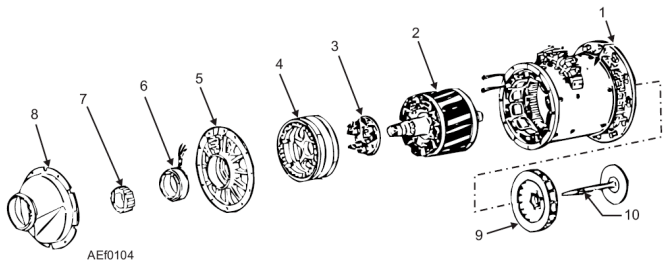

1. Stator Assembly
2. Rotor and Shaft
3. Rotating Diode Assembly
4. Exciter Rotor
5. End Bell
6. PM Generator Stator
7. Permanent Magnetic Rotor Core
8. Generator To Air Duct Adapter
9. Fan Assembly
10. Drive Shaft Assembly

Figure 1: Disassembled brushless ac generator

This paper presents the development of feature extraction and diagnostic algorithms to ultimately 1) differentiate between generator failure modes and normal aircraft operational modes; and 2) determine the degree of damage of a generator. Eventually, the algorithms will account for the GCU when determining the health of generators. This will enhance the reliability of aircraft generators by providing the maintenance personnel with information about the current health state and remaining life of generators so that timely action can be taken.

MAIN SECTION

GENERATOR HEALTH MONITORING ALGORITHMS – Figure 2 depicts the basic modules of the proposed Diagnostic and health management system architecture based upon data-driven algorithms [1][2][3] and also shows how the architecture can provide inputs to the condition-based maintenance (CBM) module for maintenance execution. The feature extraction unit takes raw sampled data from a generator and converts it to a form suitable for the diagnostic and prognostic modules. The diagnostician monitors continuously critical feature data and decides upon the existence of impending or incipient failure conditions. The detection and identification of an impending failure triggers the prognosticator. The prognosticator reports the remaining useful lifetime of the failing machine or component to the CBM module. The CBM module schedules the maintenance so that uptime is maximized while certain constraints are satisfied. The prognostic architecture is based on three constructs: 1) a static "virtual sensor" that relates known measurements to material deterioration; 2) a predictor which attempts to project the current state of the damaged material into the future thus revealing the time evolution of the damage and allowing the estimation of the material's remaining useful lifetime; and 3) a Confidence Prediction Neural Network (CPNN) [4][5] whose task is to account for uncertainty and manage/shrink the prediction bounds.

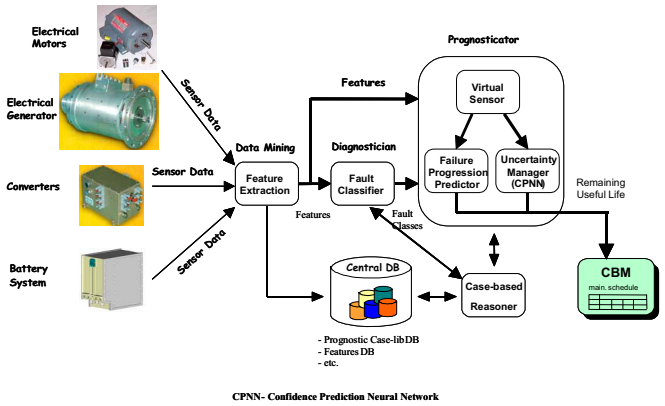

Figure 2: Overall Architecture for Diagnostic and Prognostic Assessment of Aircraft Electric Power Systems

Feature Extraction – Initial time-domain and frequency domain feature extraction algorithms have been developed to distinguish between healthy and common failure modes such as bearing failure. The time domain features (kurtosis, root mean square, etc.) and frequency domain features are calculated from (demodulated) voltage and current. These features are based upon Electrical Signature Analysis (ESA).

Each extracted feature from a set time and frequency domain based features is evaluated separately by statistical comparison with the corresponding feature database. Statistical margins are defined in order to denote the range of healthy / low-hour generators. Values outside of this range indicate the presence of a degraded / high-hour generator.

Consequently, we define the healthy operation range based on separate asymmetrical calculations of high (σ_+) and low (σ_-) margins that are calculated by generalised higher moments of features. The margins are defined for each feature separately by the following equations [6]:

$$\sigma_+ = m + s \cdot \left(\overline{\left(z_+ - m \right)^p} \right)^{1/p}$$
$$\sigma_- = m - s \cdot \left(\overline{\left(m - z_- \right)^p} \right)^{1/p} \quad (1)$$

where m denotes the median value, z_+ and z_- denote features above and below the median. The asymmetrical margins are controlled by parameters s and p which denote the stretching factor and the generalized higher moment of the feature. For a normal distribution, values s = 3 and p = 2 correspond to $\pm 3\sigma$ margins. The s value is kept at the default value s = 3 and the p value is increased to p = 4 which increases the robustness of the feature evaluation with respect to outliers in the feature space.

Demodulation – In this work, two methods are used for amplitude demodulation of voltage and current signals: (1) Hilbert transform and (2) Space vector transform. The Hilbert Transform is used on single phase quantities while the Space vector transform is applied to three-phase quantities. The goal of demodulation is to remove the dominant line frequency component contained in the phase voltage and current signals so that ripple (composed of harmonics and fault signatures) along the line frequency can be analyzed using the envelope of the raw voltage/current signals. This approach allows a clear detection of failure signatures without being swamped by the power in the line frequency [7][8]. The Hilbert transform can be expressed as follow:

$$\hat{x}(t) = \frac{1}{\pi} \int_{-\infty}^{\infty} \frac{x(\tau)}{t - \tau} d\tau \,. \quad (2)$$

The Hilbert transform creates an artificial complex signal $u(t) = x(t) + j\hat{x}(t)$ from input signal $x(t)$. The real part of the analytical signal is the original signal $x(t)$, the imaginary part $\hat{x}(t)$ represents the Hilbert transform of a real part, $x(t)$. The absolute value magnitude of the complex analytical signal forms the signal envelope and demodulates the original signal *x(t)*. The absolute value magnitude of u(t) is given by $|u(t)| = \sqrt{x^2(t) + \hat{x}^2(t)}$.

The Space vector transform creates a complex-valued one-dimensional space vector $P(t)$ from time-dependent real-valued three-phase quantities: $x_a(t)$, $x_b(t)$ and $x_c(t)$. The Space vector transform is defined as follow:

$$\begin{aligned} P(t) &= x_a(t) + \alpha \cdot x_b(t) + \alpha^2 \cdot x_c(t) \\ &= x_d(t) + j \cdot x_q(t) \end{aligned} \tag{3}$$

where $\alpha = e^{2\pi/3}$ and the d-q components are given by

$$\begin{bmatrix} x_d(t) \\ x_q(t) \end{bmatrix} = \frac{2}{3} \begin{bmatrix} 1 & -\frac{1}{2} & -\frac{1}{2} \\ 0 & -\frac{\sqrt{3}}{2} & \frac{\sqrt{3}}{2} \end{bmatrix} \begin{bmatrix} x_a(t) \\ x_b(t) \\ x_c(t) \end{bmatrix}. \tag{4}$$

The magnitude of $P(t)$, given by $|P(t)| = \sqrt{x_d^2(t) + x_q^2(t)}$, forms the amplitude demodulated signal.

Electrical Signature Analysis – ESA is the term used for the evaluation of the voltage and current waveforms. This provides an increased advantage to diagnostics as power-related, motor-related and load-related signals can be quickly compared. A key consideration when using ESA is that voltage signatures relate to the upstream of the circuit being tested (towards power generation) and current signatures relate to the downstream of the circuit being tested (towards the motor and load) as depicted in Figure 3. ESA uses the machine being tested as a transducer, allowing the user to evaluate the electrical and mechanical condition from the control or switchgear. Typically, ESA is done in the frequency domain, relying upon FFT techniques for accurate analysis [9][10][11][12]. In this work, ESA will be done in the time-domain to assess the health of generators by analyzing the amplitude demodulated signal versus phase angle of the complex signals. Frequency-domain based ESA techniques have been developed to detect and track a seeded bearing failure in a P-3 generator [9], which was not detectable in the vibration signals using visual inspection alone (no large spikes in vibration data were observed). Also the frequency-domain techniques have been used to identify the location / component of degradations in P-3 generators using available phase voltage and current waveforms.

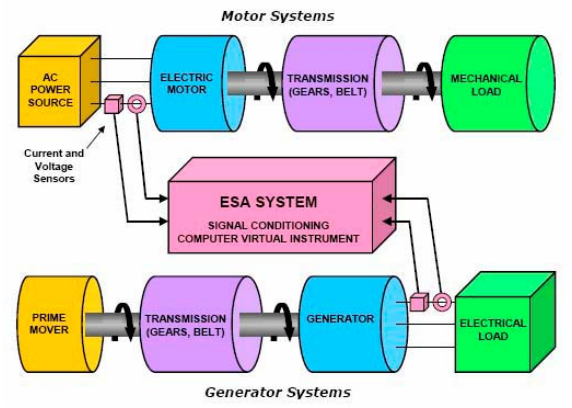

Figure 3: Applying ESA to Motor and Generator Systems

Fault Classifier – The diagnostician, implemented as a multiple-input multiple-output FNN, serves as a nonlinear discriminator to classify impending faults. The fault classifier is trained to recognize generator faults from a vector of features corresponding to rotor, stator and bearing failures.

Virtual Sensor – The virtual sensor calculates a failure measure indirectly through a neural network mapping of features and operating condition. Consider, for example, the case of an electrical generator. No direct measurement of the degree of stator / rotor winding degradation, bearings damage, etc. occurring in a generator is possible when it is in an operational state. That is, there is no such device as a "fault meter" capable of providing direct measurements of the fault evolution. The fault dimensions take the form of a vector of integer state-of-health (SOH) values where the values range from 100 (healthy) to 0 (fault).

GENERATOR CLASSIFICATION AND HEALTH ESTIMATION EXAMPLE – NAVAIR provided electrical (voltage and current) data collected at 100 kHz for five P-3 generators (Gen 73-A0255, Gen 1182, Gen 18700071, Gen 700 and Gen 765). The data was collected for the following resistive loads and operating frequency: 1) no load, 30 kVA and 60 kVA; 2) operating line frequencies of 395Hz, 400 Hz and 405 Hz. During the testing of P-3 generators at NAVAIR in 2006: Gen 18700071 was a brand new generator with 0 hours of usage, Gen 700 was identified as a high-hour generator with 2,324 hours of usage and Gen 1182 had 2,131 hours of usage. Degradations were identified in Gen 700 and Gen 1182 using frequency-domain based ESA techniques. Although no specific failure was identified for Gen 700, the total power in the odd harmonics of the line frequency was above the other generators. Gen 1182 was significantly higher than the other generators in regards to the total power in even harmonics of the line frequency and the bearing fundamental train frequency fault signature. Also, deviations from the healthy generator were observed for Gen 1182 at the stator and rotating field failure signatures.

From the collected data, analysis windows of 16,384 samples of the 3-phase voltages were demodulated using the Space vector transform of Equations (3) and (4). Figure 4 shows Space vector transform of the 3-phase voltages and the corresponding amplitude demodulated voltage signals as a function of phase angle. The minimum and maximum values of $|P(t)|$ were determined for each phase angle bin.

Diagnostic Features – As shown in Figure 4, the brand new generator has less range between the minimum and maximum values of the demodulated signal than Gen 1182. Therefore, the following two general features were selected to detect degradations in P-3 generators:

- $|P(t)|_{max\ diff} = [|P(t)|_{max} – |P(t)|_{min}]$ per phase angle bin
- $|P(t)|_{mean} = (1/N)\times\sum |P(t)|$ per phase angle bin.

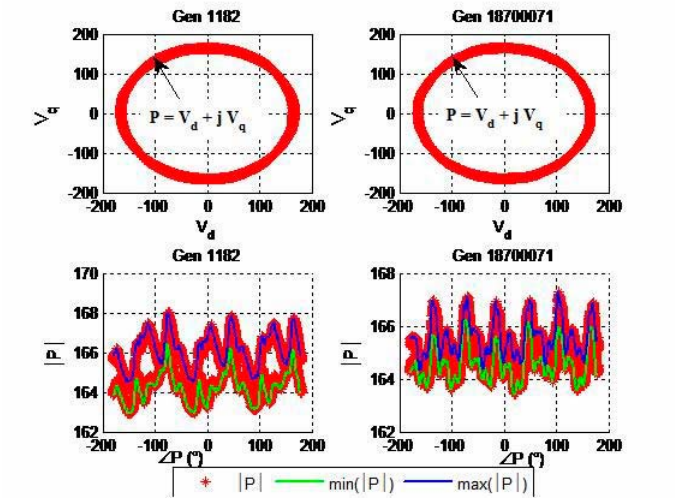

Figure 4: Demodulated Voltage signals as a function of phase angle

Comparison of Low-hour and Degraded Generators – Figures 5 through 8 shows the $|P|_{max\ diff}$ of the healthy generator versus the other four P-3 generators for all the analysis windows at 400Hz for various loads: no load, half load (30kVA) and full load (60kVA). The shape of $|P|_{max\ diff}$ is consistent for all the analysis windows containing 3-phase voltage data collected from the five the generators. Gen 73-A0255 was closest to the brand new (healthy) generator in shape and magnitude in terms of the $|P|_{max\ diff}$ feature. A slight phase shift of the feature was noticed at full load. Gen 765 was also similar to the healthy generator in shape and magnitude. The significant difference between the two generators was a more noticeable phase shift in the feature at half and full loads. Although the high hour generator (Gen 700) had a phase angle shifted shape similar to the healthy generator, it had higher peak values than the healthy generator at no load, half load and full load. Gen 1182 was significantly different from all the other generators in the shape and magnitude of the $|P|_{max\ diff}$ feature.

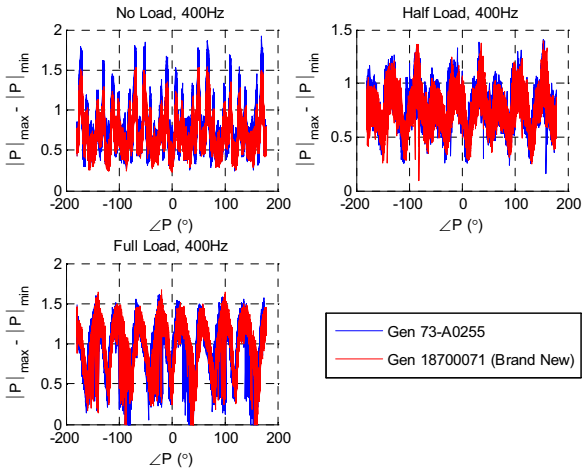

Figure 5: $|P|_{max\ diff}$ of Gen 73-A0255

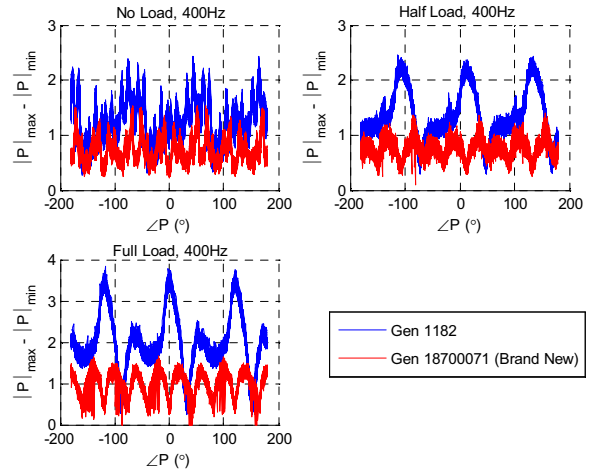

Figure 6: $|P|_{max\ diff}$ of Gen 1182

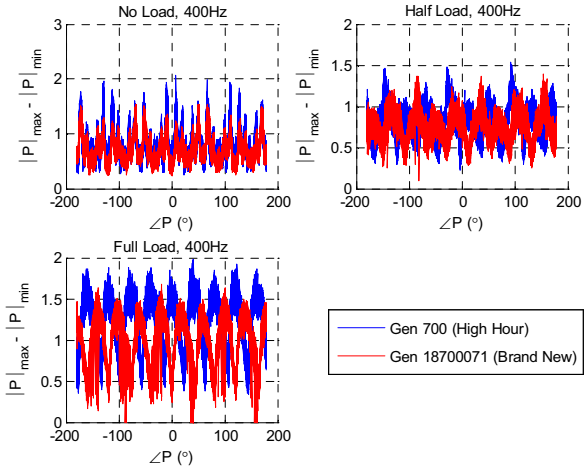

Figure 7: $|P|_{max\ diff}$ of Gen 700

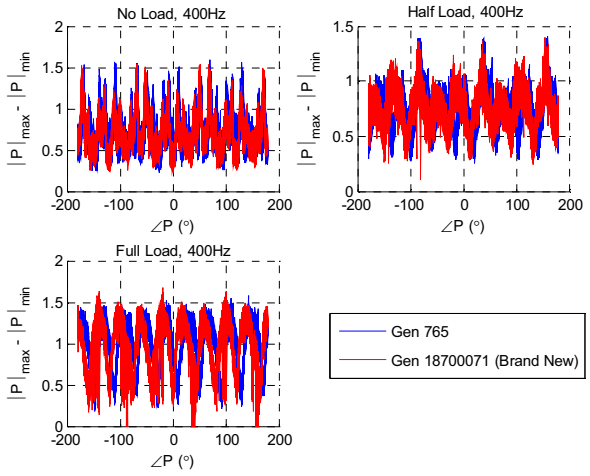

Figure 8: $|P|_{max\ diff}$ of Gen 765

Diagnostic Results – Figures 9 through 11 show polar plots of the $|P|_{max\ diff}$ feature averaged over all the analysis windows at 400Hz for the five P-3 generators at three loads (zero, half and full). As the load varied from full load to no load, the shape of the averaged $|P|_{max\ diff}$ feature changed significantly for all five generators. The generators, excluding Gen 1182, had similar shapes of the averaged $|P|_{max\ diff}$ feature for the three loads. Also, the average $|P|_{max\ diff}$ feature was able to indicate that Gen 73-A0255 is most similar to Gen 18700071, while Gen 1182 is least similar. The degradations in Gen 1182 were clearly seen at the three loads, while the degradations in the high-hour generator were easily seen at full and half loads. Therefore, the average $|P|_{max\ diff}$ feature of the healthy generator at 400Hz for no load, half load and full load were selected as load dependent reference features to compare and assess the health of all five generators.

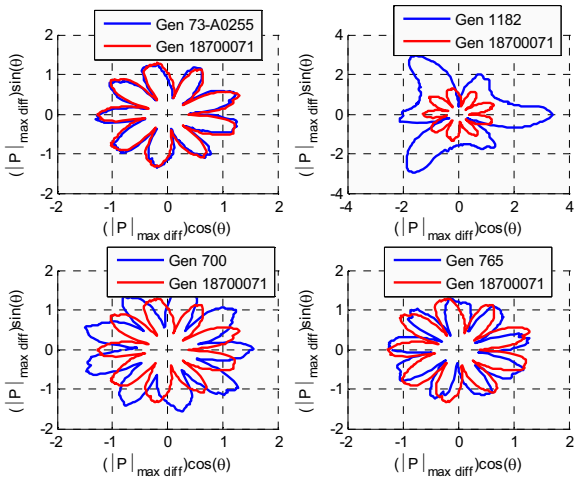

Figure 9: Average $|P|_{max\ diff}$ of Gen 18700071 versus other P-3 generators at full load

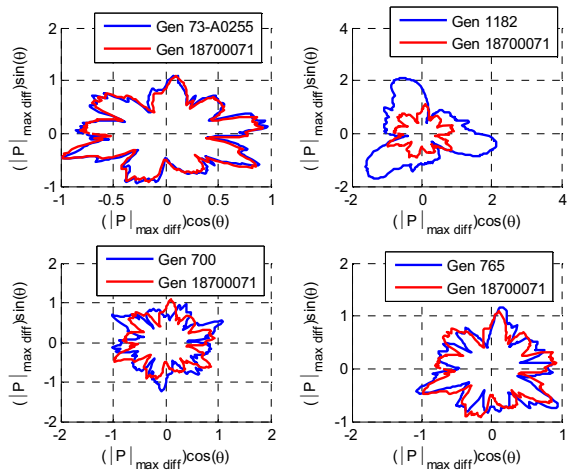

Figure 10: Average $|P|_{max\ diff}$ of Gen 18700071 versus other P-3 generators at half load

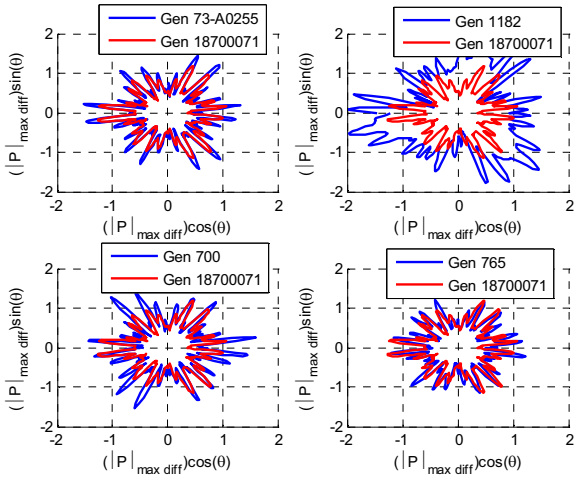

Figure 11: Average $|P|_{max\ diff}$ of Gen 18700071 versus other P-3 generators at no load

The mean absolute deviations from the reference feature, $|P|^*_{max\ diff}$, were used as an unscaled condition indicator ($CI_{unscaled}$) to differentiate between healthy and degraded P-3 generators

$$CI_{unscaled} = \frac{1}{360}\sum_{\theta=-180^\circ}^{179^\circ}\left||P|^*_{max\ diff} - |P|_{max\ diff}\right|. \quad (5)$$

Figure 12 shows the $CI_{unscaled}$ for the five generators, which varied with load and operating frequencies for the five generators. In general, the $CI_{unscaled}$ became larger as the load changed from no load to full load. The difference between the degraded generators and the healthy generator was greatest at full load. At no load or half load, the $CI_{unscaled}$ values would fail to capture the true degree of degradation in a generator. Therefore,

the $CI_{unscaled}$ must be appropriately scaled in order to accurately determine if a generator is degraded and to what degree, regardless of the operating load and frequency of the generator.

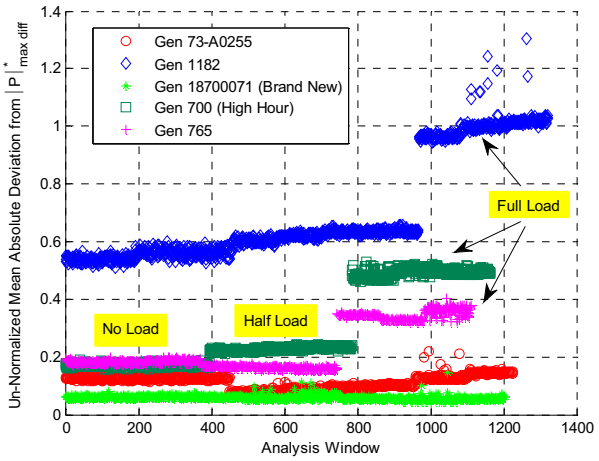

Figure 12: Unscaled condition indicator for the P-3 generators

Using $CI_{unscaled}$ data for various generators at various load and frequencies, the normalization factor, *η(load, freq)*, was calculated in the following way:

$$\eta(load, freq) = \left[\frac{1}{P}\sum_{i=1}^{P}\frac{\zeta(full\ load, 400Hz, Gen_i)}{\zeta(load, freq, Gen_i)}\right]\times \exp\left(\frac{\zeta(full\ load, 400Hz, Gen_i)}{\zeta(load, freq, Gen\,1182)}-1\right) \quad (6)$$

where Gen_i is the i^{th} generator; N_i is the number of analysis windows for the i^{th} generator; P is the number of generators; and *ζ(load, freq, Gen$_i$)* is the average of the $CI_{unscaled}$ data over the analysis windows for the i^{th} generator at a particular operating load and frequency.

The CI_{scaled} is calculated in terms of the normalization factor and $CI_{unscaled}$

$$CI_{scaled} = \eta(load, freq)\cdot CI_{unscaled} \quad (7)$$

Figure 13 shows that the normalized condition indicator for the five generators and the high (σ_+) and low (σ_-) diagnostic margins for the healthy operation range of a P-3 generator. The values of the σ_+ and σ_- margins were 0.117 and 0.036, respectively. The CI_{scaled} is more consistent for the five generators in regards to the three operating loads (no, half or full) and frequencies (395Hz, 400Hz and 405Hz). Figure 14 shows a close-up of Figure 13 with respect to the healthy generator, Gen 73-A0255 and the diagnostic thresholds.

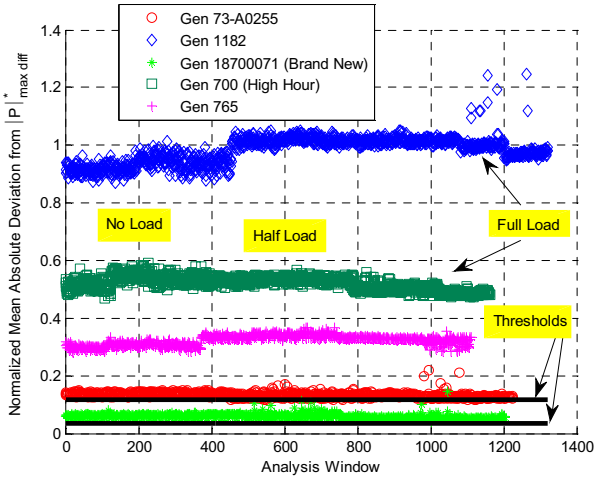

Figure 13: Scaled condition indicator for the P-3 generators

The detection rate of degradations in Gen 73-A0255, Gen 765, Gen 700 and Gen 1182 was 99.8%, 100%, 100% and 100%, respectively. The brand new P-3 generator was correctly identified as being healthy for 99.9% of the analysis windows.

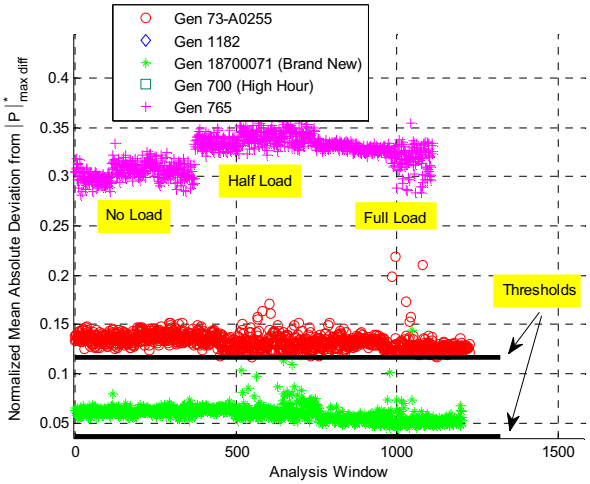

Figure 14: Closeup of scaled condition indicator for the P-3 generators

Figure 15 shows the SOH values calculated for the five generators using the following equation

$$SOH = \begin{cases} 100\dfrac{1-CI_{scaled}}{1-\sigma_+}, & if\ CI_{scaled}\in[\sigma_+, 1] \\ 100, & if\ CI_{scaled}<\sigma_+ \\ 0, & if\ CI_{scaled}>1 \end{cases}. \quad (8)$$

Further work is needed to determine how the reference feature, $|P|^*_{max\ diff}$, changes with respect to nonlinear, leading power factor and lagging power factor loads at various magnitudes.

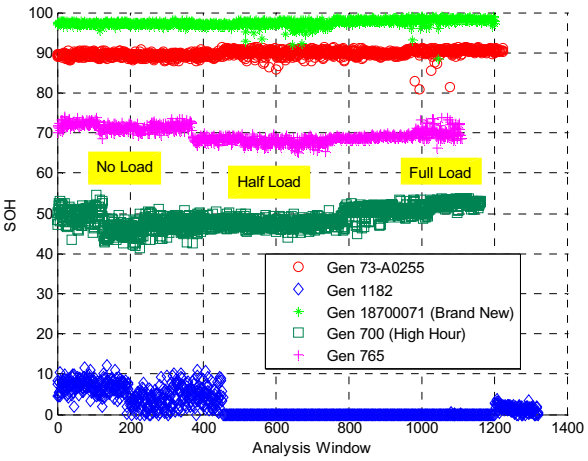

Figure 15: SOH of P-3 Generators

CONCLUSION

Time-domain features based upon ESA were developed to distinguish between healthy / low-hour and degraded / high-hour P-3 generators. Using the difference between the minimum and maximum values of the demodulated 3-phase voltage amplitude per phase angle bin, reference features ($|P|^*_{max\ diff}$) for a healthy P-3 generator were developed for various loads. The high (σ_+) and low (σ_-) margins of the CI_{scaled} (scaled mean absolute deviation from $|P|^*_{max\ diff}$) for healthy operation range were 0.117 and 0.036, respectively. The results show that the CI_{scaled} can be used to accurately detect an aircraft generator's general health and the degree of degradation. The detection rate for degraded / high-hour P-3 generators was greater than 99% with less than 0.2% false alarm rate. The brand new P-3 generator was correctly identified as being healthy for more than 99% of the analysis windows.

ACKNOWLEDGMENTS

The authors would like to thank Sean Field and Nathan Kumbar for the sponsorship of this research under NAVAIR contract number N68335-08-C-0131. In addition, the authors would like to thank NAVAIR for providing electrical and vibration test data for several low-hour and high-hour / degraded P-3 generators.

REFERENCES

1. Zhang, G., Lee, S., Propes, N., Zhao, Y., Vachtsevanos, G., Thakker, A., and Galie, T., "A Novel Architecture for an Integrated Fault Diagnostic/Prognostic System," AAAI Symposium, Stanford, California, March 25-27, 2002.
2. Wang, P. and Vachtsevanos, G., "Fault Prognosis Using Dynamic Wavelet Neural Networks," AAAI Spring Symposium, Polo Alto, March 22-24, 1999.
3. Vachtsevanos, G. and Wang, P., "A Wavelet Network Framework for Diagnostics of Complex Engineered Systems," Proceedings of MARCON 98 Maintenance and Reliability Conference, Knoxville, TN, May 12-14, 1998, (invited paper).
4. Tsui, F.C., Sun, M.G., Li, C.C., Sclabassi, R.J., "A wavelet based neural network for prediction of ICP signal", Proceedings of 1995 IEEE Engineering in Medicine and Biology 17th Annual Conference and 21 Canadian Medical and Biological Engineering, Vol. 2, pp. 1045-1046, September 20-23, 1995.
5. He, S.C. and He, Z.Y., "Blind equalization of nonlinear communication channels using recurrent wavelet neural networks", 1997 IEEE International Conference on Acoustics, Speech, and Signal Processing, Vol. 4, pp. 3305-3308, April 21-24, 1997.
6. Potocnik, P., Govekar, E., Grabec, I. and Muzic, P., "Psychoacoustic Approach to Machine Fault Diagnosis", International Journal of Acoustics and Vibration, Vol. 10, No. 3, pp. 131-136, 2005.
7. Pillay, P. and Xu, Z., "Motor current signature analysis", 1996 IEEE Industry Applications Conference, Vol. 1, pp. 587-594, October 6-10, 1996.
8. Jaksch, I. and Fuchs, P., "Rotor cage faults detection in induction motors by Motor Current Demodulation Analysis", 2007 IEEE International Symposium on Diagnostics for Electric Machines, Power Electronics and Drives, pp. 247-252, Sept. 6-8, 2007.
9. Rufus, F., Lee, S., Thakker, A., Field, S. and Kumbar, N., "Advanced Diagnostics of Aircraft Electrical Generators," SAE International Journal of Aerospace, Vol. 1, No. 1, pp. 1064-1071, 2008.
10. Penrose, H. W., "Practical Motor Current Signature Analysis Taking the Mystery Out of MCSA," ALL-TEST Pro, 2005, www.alltestpro.com/pdf/PracticalSignatureAnalysis.pdf
11. Nandi, S., Toliyat, H. A., and Li, X., "Condition Monitoring and Fault Diagnosis of Electrical Motors — A Review," IEEE Transactions on Energy Conversion, Vol. 20, No. 4, pp. 719 – 729, Dec. 2005.
12. Liu, L., "Robust Fault Detection and Diagnosis for Permanent Magnet Synchronous Motors," Phd Thesis, Florida State University, Summer 2006.

CONTACT

F. Rufus, Jr. is with Global Technology Connection, Inc., Atlanta, GA 30339 USA (phone: 770-803-3001 x29; fax: 770-234 4148; e-mail: frufus@globaltechinc.com; web address: www.globaltechinc.com).